www.setjournal.com

Electro-Osmotic Flow of MHD Jeffrey Fluid in a Rotating Microchannel by Peristalsis: Thermal Analysis

K. Venugopal Reddy¹, B. Venkateswarlu², D. Chenna Kesavaiah³, N. Nagendra⁴

¹Department of Mathematics, Anurag University, Hyderabad, T.S., India

²School of Mechanical Engineering, Yeungnam University, Gyeongsan-38541, Republic of Korea

³Basis Sciences & Humanities Vignan Institute of Technology and Science, Deshmukih, T.S., India ⁴Humanities and Sciences, Sri Sai Institute of Technology and Science, Rayachoty, A.P., India

Abstract

In this study, we examine the rotating and heat transfer on the peristaltic and electro-osmatic flow of a Jeffery fluid in an asymmetric microchannel with slip impact. A pressure gradient and anal axially imposed electric field work together to impact the electro-osmotic flow (EOF). Mathematical modeling is imported by employing the low Reynolds number and long wavelength approximation. The exact solution has been simplified for the stream function, temperature, and velocity distributions. The effects of diverse egress quantities on the gush virtue are exhibited and discussed with the help of graphs. The shear stress and trapping phenomena have been investigated. The characterization of results has been resolved for the flow governing ingrained appropriate parameters by employing the table. Our findings can be summarized as follows: (i) Debye length has a strong influence on the conducting viscous fluid of EOF in non-uniform micro-channel. (ii) The temperature field is enhanced through the elevated values of the rotation parameter and EOF. (iii) The shear stress has oscillatory behavior and the heat transmission rate increases with the magnitude of larger values of EOF. Finally, there is good agreement between the current results and those that have already been published. This model applies to the study of chemical fraternization/separation procedures and biomicrofluidic devices for the resolution of diagnosis.

Keywords: MHD, Jeffrey fluid, heat transfer, peristaltic & electroosmotic flow, asymmetric micro-channel.

1. Introduction

The electro-osmosis (EOs) method is used to create electro-osmotic flow (EOF) when electrodes are inserted into reservoirs at either end of a microchannel. The main emphasis of EOF is on the utilization of an external electric field. The interaction of electricity and electric fields leads to a change in density operating in the transverse direction, which causes bulk fluid to be propelled in a path parallel to the applied electric fields. In microfluidic devices like microreactors, DNA analyzers, biosensors, etc., EOF is essential. Ali et al. [1, 2] investigated the EDL aspect of magneto-convective trihybrid nanoparticles in the bloodstream via microtubes.

The field of medical and electronic gadgets may profit from this research. EOF simulations on MHD Jeffrey fluid in convergent geometry were demonstrated by Zubaidi et al. [3]. This study is used in medical and engineering walks to combine the fluid in difficult spots such as stimulating drugs in various veins, colliers, etc. Karmakar et al. [4] have examined the EO pumping of blood containing trihybrid nanoparticles. EOF of 3rd grad fluid due to a microchannel with magnetic field impact was examined by Nazeer et al. [5]. This study is used in microfluidic devices and biomedical systems, etc. The EO-Williamson flow on a curved surface was recently presented by Salahuddin et al. [6]. This model can be used to describe many biological fluxes that the EOF regulates.

Asghar et al. [7] inspected the EO peristaltic steam of Newtonian Ellis fluid through a dissimilar miniature channel. Narla et al. [8] and Ramesh et al. [9] investigated the EO stream of visco-elastic nanofluid due to a microchannel driven by peristaltic transfer and its applications in microscale energy devices and biomotivated EO nanofluid siphoning, etc.

The peristaltic motion of fluid often ensues in industrial and physiological appliances. The peristalsis shows a significant role in urine passage to the bladder from the kidney, food bolus and lymph, lymphatic vessels, the gastrointestinal tract, the locomotion of worms, and different other areas. Peristaltic flow across a porous wall channel was investigated by Rafig et al. [10]. This study can be applied to several physiological systems. Ali et al. [11, 12] explore the peristaltic transport of hybrid nano-blood flow in a ciliated tube. The findings of their study could be of use in the medical investigation related to diseases of organs generated in the embryonic stage, kidneys, airways, etc. Tanveer et al. [13] published work on the 2D peristaltic flow of non-Newtonian fluid through microchannels. They state that EO energy is a key fraction in reservoir engineering, the micro-fabrication process, the chemical industry, etc. Magneto-Eyring-Powell nanofluid via a non-uniform channel filled with peristalses was studied by Mallick and Misra [14]. Salahuddin et al. [15] and Ali et al. [16] scrutinized the peristaltic visco-elastic nanofluid flow in an asymmetric channel. This review is used in human physiological frameworks and found that the strain slope increases with a magnetic field, amplitudes, and volume fraction. Selvi and Srinivas [17] projected the peristaltic transport of Herschel-Bulkley liquid. Non-Newtonian nanofluids of peristaltic transport have been considered by [18-22]. The peristaltic flow of a nanofluid in a constricted artery for different shapes of nanosized particles was investigated by Devaki et al. [23].

In some physiological problems issues involving conductive fluids, such as blood pumping devices, cancer treatment, and magnetic resonance imaging for brain disorders, MHD is crucial. The EOF of magnetonanoparticles in a microtube for drug delivery applications was studied by Mondal and Shit [24]. MHD and peristaltic motion are also used in a variety of other fields, including cosmology, sensors, electronics, and magnetic medications. The EO peristaltic flow of MHD Jeffery nanofluid was published by Rafiq and coworkers [25] and found to have potential applications in food

diagnosis, drug delivery, etc. Ren et al. [26] demonstrated the EOF of MHD Jeffery fluid in parallel microchannels. The EO Enhanced MHD Third-grade fluid application for blood flow in arteries was examined by Choudhari et al. [27]. There is a ton of literature [28-30] on the EOF of MHD peristaltic motion when it is subjected to the aforementioned factors.

In some physiological problems issues involving conductive fluids, such as blood pumping devices, cancer treatment, and magnetic resonance imaging for brain disorders, MHD is crucial. The EOF of magnetonanoparticles in a microtube for drug delivery applications was studied by Mondal and Shit [24]. MHD and peristaltic motion are also used in a variety of other fields, including cosmology, sensors, electronics, and magnetic medications. The EO peristaltic flow of MHD Jeffery nanofluid was published by Rafiq and coworkers [25] and found to have potential applications in food diagnosis, drug delivery, etc. Ren et al. [26] demonstrated the EOF of MHD Jeffery fluid in parallel microchannels. The EO Enhanced MHD Third-grade fluid application for blood flow in arteries was examined by Choudhari et al. [27]. There is a ton of literature [28-30] on the EOF of MHD peristaltic motion when it is subjected to the aforementioned factors.

The study of heat transfer (HT) plays a major role in many important purposes in industry and medicine. An essential area of study is how HT affects the human body. Heat is transferred by a variety of mechanisms, including tissue conduction, arterial-venous blood perfusion through tissue pores, and more. The HT of EOF on MHD non-Newtonian fluid in a rotating microfluidic channel was investigated by Siva et al. [31]. Noreen et al. [32, 33] analytically the examined HT of **MHD** Carreau/Williamson fluid via an asymmetric/microchannel with peristalsis. The study applies to the design of peristaltic-MHD blood-micro pumps, DNA chips, food diagnostics, smart sensors, etc. The HT investigation of the EOF of Williamson fluid in a microchannel was studied by Imran et al. [34]. Deng et al. [35] and Sun et al. [36] published the work on HT in the EOF of nanofluids via a microchannel/tube and the study used in electronics cooling, microfluidics, microsystems, thermal combinations, etc. HT of hybrid nanofluids was presented by Venkateswarlu and Co [37, 38] and it was found that the HT of hybrid nanofluids is higher than that of mono nanofluids. Efforts have been

made on peristalsis with the mixed impact of mass and HT for different researchers [39–44].

The study of heat transfer (HT) plays a major role in many important purposes in industry and medicine. The human body with HT is a significant area of research, and the application of heat happens as conduction in tissues, perfusion arterial-venous blood through the pores of the tissue, etc. The HT of EOF on MHD non-Newtonian fluid in a rotating microfluidic channel was investigated by Siva et al. [31]. Noreen et al. [32, 33] analytically examined the HT of MHD Carreau/Williamson fluid via an asymmetric/microchannel with peristalsis. The study applies to the design of peristaltic-MHD blood-micro pumps, DNA chips, food diagnostics, smart sensors, etc. The HT investigation of the EOF of Williamson fluid in a microchannel was studied by Imran et al. [34]. Deng et al. [35] and Sun et al. [36] published the work on HT in the EOF of nanofluids via a microchannel/tube and the study in electronics cooling, microfluidics, microsystems, thermal combinations, etc. HT of hybrid nanofluids was presented by Venkateswarlu and Co [37, 38] and it was found that the HT of hybrid nanofluids is higher than that of mono nanofluids. Efforts have been made on peristalsis with the mixed impact of mass and HT for different researchers [39–44].

The rotation principle applies to geophysical and cosmic flows. The presence of rotation is used to study the behavior of ocean circulation and galaxies formation. The analysis of the energy transitions between quantized rotational states of particles in the gaseous phase through rotation. Because of this, many investigations have been done by many researchers [45-47]. Patel et al. [48] scrutinized the EO behavior of power-law fluid flow in a rotating microchannel. This research is important in the design of a CD system with delicate channels for handling bio-liquids such as blood, spit/mucus, and so on. Rotating the EOF via a microchannel was examined by Xu and Jian [49]. Liang et al. [50] imposed the finite difference scheme for the EOF of Oldroyd-B fluid in a rotating microchannel. It is found that the rotating EOF of Oldroyd-B liquid requires a restricted unwinding time to arrive at a moderately steady state, and the wavering at the focal point of the microchannel is more prominent than that close to the divider. Rotating the EOF of 2nd order fluid in a microchannel was inspected by Cao et al. [51], and it was accomplished that the streamwise speed built initially and declined after the consistent stream comes to by the presence of precise speed. The rotating flow of

magneto-micro/nanofluid was investigated by Narayana and association [52–54].

A review of related literature shows that nobody of the previous investigators has studied the peristaltic flow of Jeffrey fluids. We have attempted to develop a mathematical model that accounts for the effects of rotation, slip, Joule heating, and EO flow in light of the foregoing. The analytical solutions for stream function, velocity distribution, heat transfer distribution, and also flow behaviors have been analyzed. The results are presented graphically for interpreting them with ease.

2. Mathematical formulation

We measured the 2D EO peristaltic transport and HT of an incompressible, viscous fluid over an asymmetric micro-channel with negatively charged walls, as shown in Figure 1. It is presumable that the flow is asymmetric around X, and that the liquid is moving along the X path. The hydrophobic micro-channel is enclosed by gradually differing ramparts at $h_1(X) = Y = h_2(X)$ which the distance end-to-end of the channel (L) is implicitly assumed to be frequently better than the height, i.e. $(h_1 + h_2) << L$.

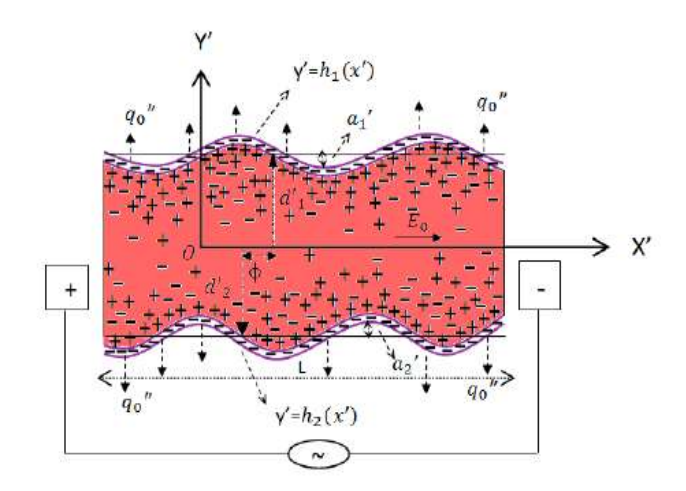


Figure 1. Problem sketch

The wavy channels' geometrical form is specified as

$$d_1' + \cos\left(\frac{2\pi X}{L}\right) a_1' = h_1'(X) \text{ and}$$

$$d_2' + \cos\left(\frac{2\pi X}{L} + \phi\right) a_2' = -h_2'(X)$$
(1)

2.1. Electrical model

The primary studies of electrostatics are associated with the Poisson-Boltzmann equation for the electrolyte symmetric given by

$$\frac{d^2\psi'(Y)}{dY^2} = \frac{2n_0ez_v}{\varepsilon}\sinh\left(\frac{ez_v\psi'(Y)}{k_BT_{av}}\right)$$
(2)

where η_o , ε , z_v , e, k_B , T_{av} , ρ_e and ψ' are the ions concentration, proton charge, ions valence, medium permittivity, Boltzmann constant, net electric charge density, Poisson-Boltzmann equation, and the boundary setting for potential function are represented as

$$\psi'_1 = \psi'(Y) \text{ and } \psi'_2 = \psi'(Y) \text{ at}$$

 $\psi'_1 = \psi'(Y), h'_1(X) = Y = h'_2(X)$
(3)

where ψ'_1 and ψ'_2 are the electrical potential at the lower and upper walls.

The non-dimensional variables have been introduced as the following equations

$$x = \frac{X}{L}, y = \frac{Y}{d_1'} \quad \text{and}$$

$$\left[\psi_O, \psi_1, \psi_2\right] = \frac{ez_v}{k_B T_{ov}} \left[\psi', \psi_1', \psi_2'\right]$$
(4)

Eqns. (1) and (2), we get the subsequent form given as

$$h_1(x) = \frac{h_1'}{d_1'} = 1 + a_1 \cos(2\pi x)$$
 (5)

$$h_2(x) = \frac{h_2'}{d_1'} = -d - a_2 \cos(2\pi x + \phi)$$
 (6)

$$\frac{d^2 \psi_O}{dv^2} = k^2 \sinh\left(\psi_O\right) \tag{7}$$

where

$$a_1 = \frac{a_1'}{d_1'} a_2 = \frac{a_2'}{d_1'} d = \frac{d_2'}{d_1'} k = \frac{d_1'}{\lambda}$$

are described as the electro-osmotic parameter, λ is the EDL thickness which is inversely proportional to the

electro-osmotic parameter and is designed by $\frac{1}{\lambda} = \left(\frac{2n_o e^2 z_v^2}{\varepsilon k_B T_{av}}\right)^{\frac{1}{2}}$

The non-layered type of limit conditions characterized in (3) utilizing the dimensionless factors (4) diminish to

$$\psi_1 = \psi_o(y)$$
 and $\psi_2 = \psi_o(y)$ at
$$h_1(x) = y = h_2(x)$$
 (8)

We pick that the warm potential is a lot higher than the electric potential which the Hiickel-Debye linearization rule preserves $\sim x \approx \sinh(x)$. Based on this presumption, the arrangement of Poisson-Boltzmann condition (7) take in the structure as

$$\frac{d^2\psi_o}{dv^2} = k^2\psi_o \tag{9}$$

The closed structure arrangement of the situation (9) is obtained by using the boundary conditions (8) gives rise to

$$\psi_o(y) = F_1 \cosh(ky) + F_2 \sinh(ky) \tag{10}$$

2.2. Jeffrey Fluid model

The basic equations for an incompressible Jeffrey fluid are

$$T = -pI + S$$
 and $S = \frac{\mu}{1 + \lambda_1} (\dot{\gamma} + \lambda_2 \ddot{\gamma})$ (11)

where p, I, λ_1 , λ_2 , $\dot{\gamma}$ and S are the pressure, identity tensor, relaxation ratio to retardation times, rate of shear, and extra stress tensor for Jeffrey fluid.

The relevant field equations that describe the flow of fluid in the laboratory frame are provided as

$$\frac{\partial u^*}{\partial x} = -\frac{\partial v^*}{\partial y} \tag{12}$$

$$\rho \left\{ \frac{\partial}{\partial t} + u^* \frac{\partial}{\partial x} + v^* \frac{\partial}{\partial y} \right\} (u^*) - 2\rho \Omega v^* = -\frac{\partial P}{\partial x}$$

$$+ \frac{\partial}{\partial x} (S_{xx}) + \frac{\partial}{\partial y} (S_{xy}) - \sigma B_0^2 u^* + \rho_e \overline{E}$$
(13)

$$\rho \left\{ \frac{\partial}{\partial t} + u^* \frac{\partial}{\partial x} + v^* \frac{\partial}{\partial y} \right\} (v^*) + 2\rho \Omega u^* = -\frac{\partial P}{\partial y} + \frac{\partial}{\partial x} (S_{xy}) + \frac{\partial}{\partial y} (S_{yy})$$
(14)

$$c_{p} \left\{ \frac{\partial}{\partial t} + u^{*} \frac{\partial}{\partial x} + v^{*} \frac{\partial}{\partial y} \right\} (T) = \frac{K}{\rho} \nabla^{2} T$$

$$+ \gamma \Phi + \frac{\sigma B_{0}^{2} u^{*2}}{\rho} + \frac{\sigma E^{2}}{\rho}$$
(15)

where
$$\nabla^2 = \frac{\partial^2}{\partial x^2} + \frac{\partial^2}{\partial y^2}$$
, $P = p - \frac{1}{2}R^2\Omega^2\rho$

$$\Phi = \frac{1}{1 + \lambda_1} \left\{ 1 + \lambda_2 \left(u^* \frac{\partial}{\partial x} + v^* \frac{\partial}{\partial y} \right) \right\}.$$

$$\left\{ 2 \left(\frac{\partial u^*}{\partial x} \right)^2 + 2 \left(\frac{\partial v^*}{\partial y} \right)^2 + \left(\frac{\partial u^*}{\partial y} + \frac{\partial v^*}{\partial x} \right)^2 \right\}$$
(16)

The slip conditions of velocity (Navier-Slip) at the solid-fluid edge are (see Ref. [44]) by

$$u^* = -b_1 \frac{du^*}{dy}$$
 and $u^* = b_2 \frac{du^*}{dy}$ at
 $h_1'(x) = y = h_2'(x)$ (17)

where b_2 & b_1 are the lengths of the wall channels $h_2' = y = h_1'$.

$$\overline{u} = \frac{u^*}{U_{HS}} \qquad U_{HS} = -\frac{\varepsilon E_o k_B T_{av}}{e z_v \mu}$$

Assent to U_{HS} , $ez_{\nu}\mu$ the classical osmotic-electro motion velocity of the microchannel in the absence of velocity slip, (u^*, v^*) : velocity components along the paths (x, y), Ω : rotation vector, σ : electric conductivity, K: thermal conductivity. In the Laboratory framework of alteration, equations are appropriated as

$$\overline{u} = u^* - c, \quad \overline{v} = v^*, \quad \overline{x} = x - ct,$$

$$\overline{y} = y, \quad \overline{p}(\overline{x}) = P(x, t)$$
(18)

where $(\overline{u}, \overline{v})$: the velocities of wave frames concerning $(\overline{x}, \overline{y})$ and (P, \overline{p}) : the fixed frame of references and wave pressures.

The suitable dimensionless variables for the motion were designed as

$$h_{1} = \frac{h'_{1}}{d'_{1}}, \quad h_{2} = \frac{h'_{2}}{d'_{1}}, \quad S = \frac{d'_{1}S}{\mu c}, \quad u^{*} = \frac{\overline{u}}{c}$$

$$v^{*} = \frac{\overline{v}}{c\delta}, \quad \delta = \frac{2\pi d'_{1}}{\lambda_{1}}, \quad p = \frac{2\pi d'_{1}^{2}\overline{p}}{\mu c\lambda_{1}}$$

$$t = \frac{2\pi c\overline{t}}{\beta}, \quad d = \frac{d'_{2}}{d'_{1}}, \quad M = \sqrt{\frac{\sigma}{\mu}}B_{0}d, \quad a = \frac{a'_{1}}{d'_{1}}$$

$$b = \frac{a'_{2}}{d'_{1}}, \quad d = \frac{d'_{2}}{d'_{1}}, \quad A = \frac{\sigma\overline{E}^{2}d'_{1}^{2}}{\rho v c_{p}(T_{1} - T_{0})}$$

$$Re = \frac{cd'_{1}}{v}, \quad \theta = \frac{T - T_{0}}{T_{1} - T_{0}}, \quad R = \frac{\Omega}{\mu}a^{2}, \quad \beta_{1} = \frac{b_{1}}{d'_{1}}$$

$$Ec = \frac{c^{2}}{c_{p}(T_{1} - T_{0})}, \quad \Pr = \frac{\rho v c_{p}}{K}, \quad \beta_{2} = \frac{b_{2}}{d'_{1}}$$

$$C_{o} = \frac{d'_{1}^{2}}{\mu U_{HS}} \left(-\frac{d\overline{p}}{dx}\right)$$

The non-dimensional stream function $\psi(x,y)$ is applied such that

$$u = \frac{\partial \psi}{\partial v}$$
 and $v = -\delta \frac{\partial \psi}{\partial x}$ (20)

By using (17)–(19) and under the creeping flow approximation, the Eqns. (11)–(15) are reduced into

$$\left(\frac{1}{1+\lambda_1}\right)\frac{\partial^4 \psi}{\partial y^4} + \left(R - M^2\right)\frac{\partial^2 \psi}{\partial y^2} + \frac{d^3 \psi_o}{dy^3} = 0$$
 (21)

$$\frac{1}{\Pr} \frac{\partial^2 \theta}{\partial y^2} + \frac{Ec}{(1+\lambda_1)} \left(\frac{\partial^2 \psi}{\partial y^2} \right)^2 + M^2 \left(\frac{\partial \psi}{\partial y} \right)^2 + A = 0$$
(22)

The associated boundary conditions of the stream function and temperature are formed as

$$\psi = \frac{q}{2}, \quad \frac{\partial \psi}{\partial y} + \frac{\beta_1}{1 + \lambda_1} \frac{\partial^2 \psi}{\partial y^2} = -1 \quad \text{at}$$

$$y = h_1(x) = 1 + a \cos[x]$$
(23)

$$\psi = -\frac{q}{2}, \frac{\partial \psi}{\partial y} - \frac{\beta_2}{1 + \lambda_1} \frac{\partial^2 \psi}{\partial y^2} = -1 \text{ at}$$

$$y = h_2(x) = -d - b \cos[2\pi x + \varphi]$$
(24)

$$\theta = 0$$
 at $y = h_1$ and $\theta = 1$ at $y = h_2$ (25)

where M, \Pr{Ec} , λ_1 , R, ϕ , L and q are the Hartmann number, \Pr{Cc} randtl number, P ckert number, P Material parameter, rotation parameter, phase difference, slip parameter, and the flux in the wave frame.

3. Method of clarification

The closed explanation of Eq. (21) among the borderline setting (23)-(24) is given by

$$\psi = C_1 + C_2 y + C_3 \cosh(Ny) + C_4 \sinh(Ny) + F_3 y^2 + F_4 \cosh(ky) + F_5 \sinh(ky)$$
(26)

The solution of axial velocity is obtained as

$$\frac{\partial \psi}{\partial y} = u = C_2 + C_3 N \sinh(Ny) + C_4 N \cosh(Ny) + 2F_3 y + F_4 k \sinh(ky) + F_5 k \cosh(ky)$$
(27)

The solution of temperature Eqn. (22) using Eqn. (26) associated with Eqn. (25) is obtained as

$$\theta = C_5 + C_6 y + G_{50} + G_{51} + G_{52} \tag{28}$$

The stress of shear is stated as

$$s_{xy} = \frac{1}{1 + \lambda_1} \frac{\partial^2 \psi}{\partial y^2} \Longrightarrow s_{xy} = \frac{1}{\left(1 + \lambda_1\right)} G_{56}$$
 (29)

The heat transfer coefficient is given by

$$Nu = -\frac{\partial \theta}{\partial y}\Big|_{y=h_1,h_2}$$

$$\Rightarrow Nu = -\left(G_{53} + G_{54} + G_{55}\right)$$
(30)

The Appendix A contain explanations.

4. Results and discussion

The main purpose of this portion is to analyze the impact of involved quantities on the function of stream (ψ) , axial velocity (u), temperature (θ) , coefficients of heat transfer (Nu), and shear stress (S_{xy}) . The constants are set for any numerical calculations that are not specified in the graph, such as a=0.4, b=0.9, $\phi=\frac{\pi}{3}$, $\lambda_1=A=1.5$, R=3.5, M=3.0, Q=2.0, $\beta_1=0.03$, $\beta_2=0.02$, $C_o=0.1$, d=Ec=k=Pr=1.0 and $\psi_1=\psi_2=0.3$. Finally, Table 1 exhibits the comparison with already presented results by considering k=0 it as a special case of our study. We can inspect from Table 1 that the current results are in very good accord with the Mondal and Shit [44].

Table 1. Variation of u with y for different values of M when $\beta_1 = 0.03$, $\beta_2 = 0.02$, $\psi_1 = \psi_2 = 0.2$

y	M = 3.0	M = 3.2	M = 3.4
-0.5873	-0.9593	-0.9568	-0.9543
-0.0873	0.1859	0.1814	0.1767
0.4127	0.3015	0.2803	0.2611
0.9127	-0.0447	-0.0297	-0.0164

4.1. Velocity profile

The axial speeds determinedly show parabolic profiles, exhibiting that likewise with simply the flow of the viscous laminar channel. The greatest speed emerges at the channel centerline (for example at the best separation from the channel dividers, where friction is higher). Figures B2(a)–B2(f) illustrate the effects of M, λ_1 , R, k, β_1 and β_2 on the fluid velocity. Illustrated Figure B2(a) detected that the velocity profile reduces due to an increase in M and the strength of Lorentz is protection in nature. The impacts of λ_1 and R on liquid velocity are shown in Figure B2(b) and Figure B2(c), and it is clear that the velocity field improves with higher values of λ_1 and R. The temperature rises as a result of raising the radiation parameter R-value. The R process

produces more heat, which enhances the temperature field.

Figure B2(d) visualizes the influence EO parameter on axial velocity. There is a progressive reduction in axial flow with increasing EO parameter with greater transverse coordinates. Decreasing Debye length, therefore, results in a damping in the axial flow. The deceleration is induced by the electrokinetic body force. This damping is generally sustained quite strongly except for higher values of transverse coordinate where the upper microchannel wall is approached and the reverse trend is observed here i.e. acceleration in the axial flow. **Figure B2(e) and Figure B2(f)** accounts for the slip effect on velocity distribution. As the slip gets large the velocity rises near the boundaries whereas the overall effect of slip on *u* is increasing.

Figure B2(d) analyzes that the axial velocity rises with an enhancement in the EO variable k. As the electro-osmotic specification is complementary of EDL after that as enlarging k, the EDL thickness diminishes thereby bulk fluid flow rises. The osmotic-electro speed u is higher for some signs k in the middlemost area of the channel. It demonstrates that an expansion in the stature of the microchannel and reduction in the Debye thickness causes an ascent in axial speed. **Figure B2(e) and Figure B2(f)** depict that the impact of different slip parameters β_1 and β_2 on the velocity profile. It is found that the velocity is radically climbed at the lower wall than that of the upper wall of the channels.

4.2. Temperature profile

Figures B3(a)-B3(g) show the impact of M, λ_1 , R, k, A, β_2 and Pr on fluid hotness. Figure B3(a) highlights that for upgrading the size M, the behavior of temperature decreases. Figure B3(b) Figure B3(c) show the effects on λ_1 and R on the heat profile. It is observed that the heat worth enhances through the higher values of λ_1 and R. The inspiration k on the thermal field is represented in Figure B3(d), we can notice that an increase k affects the thermal field augmentation.

Figure B3(e) shows an essential outcome of Pr on the temperature profiles. It is noticed that the Brinkman quantity has an impulse to diminish the hotness in the micro-channel. It might be inferred that the fluid thermal

conductivity decays by improving the Prandtl quantity. Since Pr is the ratio between momentum diffusivity and thermal diffusivity, the higher the velocity, the greater the Prandtl-enhanced temperature that will result. **Figure B3(f)** depicts that the temperature enhances when the effect of the slip parameter β_2 increases. According to **Figure B3(g)**, the liquid's hotness increases in direct proportion to a rise in Joule heating at the center of the channel, while it decreases near the wall.

4.3. Nusselt number

Figures B4(a)-B4(h) depict the impact of sundry parameters such as M , R , k , Pr , Ec , β_1 and β_2 correspondingly on the size of heat convey coefficient. Figure B4(a) represents that the heat transfer rate increases for larger Hartmann numbers. The graphical results of the heat transfer rate are oscillatory in nature as a consequence of peristaltic activity at the walls. Figure **B4(b)** shows that the heat transfer coefficient depresses for larger values of the rotation parameter. It is noted that a larger EO number enhances the Nusselt number while opposite behavior is observed with the effect of pressuredriven osmotic parameter from Figure B4(c) and Figure B4(d). Figure B4(e) represents the heat transfer coefficient diminishes as the magnitude of larger values of the Prandtl number while the heat transfer coefficient rises when the increasing the values of the Eckert number from Figure B4(f). From Figures B4(g) and Figure **B4(h)**, we can notice that an increase in β_1 and β_2 affects the heat transfer coefficient depresses.

4.4. Shear stress

The pivotal shear stress appropriation (S_{xy}) on the topsy-turvy (i.e. asymmetric) channel upper wall for various upsides of (M), (λ_1) , (b), (Q), (Ω) and (ϕ) are presented in **Figures B5(a)-B5(f)**. The **Figures B5(a)-B5(f)** portrays that an absolute worth of the stress of shear upgrades with expanding of M, λ_1 , b, Q, Ω and ϕ . The stress behavior is in oscillatory which might be because of peristalsis. In addition, the absolute upsides of shear pressure are bigger if there should be an occurrence of a Jeffery liquid when compared to Newtonian liquid.

4.5. Trapping phenomenon

The captivating quality in fluid motion is demonstrated by the plotting of streamlines in **Figures B6(a)-B6(d)**. A bolus is confined when a smooth-out is split under particular conditions, and it is transported along with the wave in the wave pattern-this process is referred to as a trap. **Figure B6(a) and Figure B6(b)** show that the caught bolus is found to grow by improving M and consequently, the bolus size depressing with ascending of λ_1 which is exposed in **Figure B6(c) and Figure B6(d)**.

5. Conclusions

Motivated by novel investigations in osmotic-electro micro-pumps an innovative mathematical representation has been conferred for the analysis of heat transmit on magneto peristaltic and electro-osmotic motion of a rotating Jeffrey fluid in an unsymmetrical micro-channel. Using approximations of creeping flow, the modeled equations have been interpreted. Closed-form solutions have been derived for stream function, axial velocity, temperature, Nusselt number and Shear stress. The behaviors of stream aspects are inspected through plots. Our results can be reviewed as:

- The length of Debye is firmly dominated by the fluids of viscous conducting EOF within a non-uniform microchannel.
- As increasing in rotation parameter, the temperature field enhances.
- The temperature rises as the higher values of EOF.
- The Nusselt number increases as the magnitude of larger values of EOF.
- The Shear stress has oscillatory behavior.

Nomenclature

Symbol Description

 (a_1, a_2) the left and right amplitude of micro-asymmetric vessel (m)

(b,a) dimensionless right and left amplitude of microasymmetric vessel

c speed of the wave (m/s)

 C_p specific heat ability $(J/(kg. K))(Kelvin^{-1}sec^{-2}m^2)$

 $\left(C_0,C_1\right)$ solutal concentration at the left and right walls respectively

 \bar{C} solutal concentration

d width of $\frac{1}{2}$ the channel (m)

 E_{x} applied field of electrical

 \overline{E} potential of electric

E dimensionless electric potential

e primary charge

F mean flows

Gr Grashof number

g acceleration due to gravity (ms^{-1})

k' permeability of porous walls (Darcy quantity) (W/mKelvin)

 k^* coefficient of mean absorption (m^{-1})

L slip variable

 m^2 micro polar parameter

n coupling number

 (\overline{p}, p) dimensional, & dimensionless pressures $(kg/m.s^2)$

Pr Prandtl number

 \overline{q}_r the radiative flux of unidirectional

 \overline{Q}_0 dissipation function $(kgm^{-1}sec^{-3})$

Rn parameter of radiation

Re Reynolds quantity

t time (sec)

 \overline{T} temperature (*Kelvin*)

 T_m average temperature (*Kelvin*)

 (T_0, T_1) the temperature at the left and right walls (*Kelvin*)

 $U_{H\!S}$ velocity of Smoluchowski-Helmholtz

 $(\overline{u}, \overline{v})$ wave frame velocity components of $(\overline{x}, \overline{y})$ (m sec^{-l})

- $(\overline{U},\overline{V})$ ixed frame velocity components of $(\overline{X},\overline{Y})$
- (u,v) dimensionless velocity components of (x,y)

Greek symbols

- ho_0 nanofluid density at the reference temperature (T_0) (kg/m^3)
- ρ_p nanoparticle mass density (kg/m^3)
- ρ_f nanoparticle fluid density (kg/m^3)
- $\overline{\rho}_{a}$ electric charge density
- μ fluid viscosity($kg m^{-1} sec^{-1}$)
- k_v kinematic rotational viscosity ($m^2 sec^{-1}$)
- λ wavelength(m)
- 2 Jeffrey fluid parameter
- β_t fluid volumetric thermal expansion (1/Kelvin)
- β_c fluid volumetric solutal expansion (m^3/kg)
- K_{ef} thermal conductivity (W/(m. K)),
- σ^* constant of Boltzmann-Stefan ($W m^{-2} Kelvin^{-4}$)
- ε medium dielectric permittivity (Fm^{-1})
- ς potential of zeta (v)
- ϕ difference of phase
- σ concentration of solute
- $\alpha_{\scriptscriptstyle m}$ thermal diffusivity
- α' coefficient of slip at the porous surface walls
- β parameter of heat source/sink
- Θ average flux of time
- γ volume fraction of nanoparticle
- K parameter of osmotic-electro-osmotic
- Ω axial velocity of micro rotation
- θ dimensionless temperature

- ψ stream function
- δ wave number

Funding

The authors received no financial support for the research, authorship and publication of this article.

Conflicts of interests/Competing interests

The authors declared no potential conflict of interest concerning the research, authorship, and publication of this article.

Data Availability

The data sharing does not apply to this article as no datasets were generated or analyzed during the current study.

References

- [1] A. Ali, A. Barman, and S. Das, "EDL aspect in ciliaregulated bloodstream infused with hybridized nanoparticles via a microtube under a strong field of magnetic attraction," *Thermal Science and Engineering Progress*, vol. 36, p. 101510, 2022.
- [2] S. Das, A. Ali, R. N. Jana, and O. D. Makinde, "EDL impact on mixed magneto-convection in a vertical channel using ternary hybrid nanofluid," *Chemical Engineering Journal Advances*, vol. 12, p. 100412, 2022.
- [3] A. A. Zubaidi, M. Nazeer, G. S. Subia, F. Hussain, S. Saleem, and M. M. Ghafar, "Mathematical modeling and simulation of MHD electro-osmotic flow of Jeffrey fluid in convergent geometry," *Waves in Random and Complex Media*, 2021.
- [4] K. Karmakar, A. Ali, and S. Das, "Circulation of blood loaded with trihybrid nanoparticles via electro-osmotic pumping in an eccentric endoscopic arterial canal," *International Communications in Heat and Mass Transfer*, vol. 141, p. 106593, 2023.
- [5] M. Nazeer, F. Hussain, M. I. Khan, A. Ur Rehman, E. R. El Zahar, Y. M. Chu, and M. Y. Malik, "Theoretical study of MHD electro-osmotically flow of third-grade fluid in micro channel," *Applied Mathematics and Computation*, vol. 420, p. 126868, 2022.
- [6] T. Salahuddin, I. Kousar, and M. Khan, "An electroosmotic Williamson flow analysis by means of curved

- surface," *Materials Science and Engineering: B*, vol. 290, p. 116221, 2023.
- [7] Z. Asghar, M. Waqas, M. A. Gondal, and W. A. Khan, "Electro-osmotically driven generalized Newtonian blood flow in a divergent micro-channel," *Alexandria Engineering Journal*, vol. 61, no. 6, pp. 4519–4528, 2022.
- [8] V. K. Narla, D. Tripathi, and O. A. Beg, "Electro-osmotic nanofluid flow in a curved microchannel," *Chinese Journal of Physics*, vol. 67, pp. 544–558, 2020.
- [9] K. Ramesh, D. Tripathi, M. M. Bhatti, and C. M. Khalique, "Electro-osmotic flow of hydromagnetic dusty viscoelastic fluid in a microchannel propagated by peristalsis," *Journal of Molecular Liquids*, vol. 314, p. 113568, 2020.
- [10] A. M. Rafiq, A. Shaheen, Y. Trabelsi, S. M. Eldin, M. I. Khan, and D. K. Suker, "Impact of activation energy and variable properties on peristaltic flow through porous wall channel," *Scientific Reports*, vol. 13, p. 3219, 2023.
- [11] A. Ali, A. Barman, and S. Das, "Electromagnetic phenomena in cilia actuated peristaltic transport of hybrid nano-blood with Jeffrey model through an artery sustaining regnant magnetic field," *Waves in Random and Complex Media*, 2022.
- [12] A. Ali, R. N. Jana, and S. Das, "Significance of entropy generation and heat source: the case of peristaltic blood flow through a ciliated tube conveying Cu-Ag nanoparticles using Phan-Thien-Tanner model," *Biomech. Model. Mechanobiol.*, 2021.
- [13] Tanveer, S. Mahmood, T. Hayat, and A. Alsaedi, "On electroosmosis in peristaltic activity of MHD non-Newtonian fluid," *Alexandria Engineering Journal*, vol. 60, no. 3, pp. 3369–3377, 2021.
- [14] Mallick and J. C. Misra, "Peristaltic flow of Eyring-Powell nanofluid under the action of an electromagnetic field," *Engineering Science and Technology, an International Journal*, vol. 22, no. 1, pp. 266–281, 2019.
- [15] T. Salahuddin, M. H. U. Khan, M. Arshad, M. A. A. Sattar, and Y. Elmasry, "Peristaltic transport of heat and mass in an asymmetric channel," *Journal of Materials Research and Technology*, vol. 9, no. 4, pp. 8337–8349, 2020.
- [16] A. Ali, M. Awasin, A. Al Zubaidi, S. Saleem, and D. N. K. Marwat, "Hartmann boundary layer in peristaltic flow for viscoelastic fluid: Existence," *Ain Shams Engineering Journal*, vol. 13, no. 2, p. 101555, 2022.
- [17] C. K. Selvi and A. N. S. Srinivas, "Peristaltic transport of Herschel-Bulkley fluid in a non-uniform elastic tube," *Propulsion and Power Research*, vol. 8, no. 3, pp. 253– 262, 2019.
- [18] M. Rashid, K. Ansar, and S. Nadeem, "Effects of induced magnetic field for peristaltic flow of Williamson fluid in a curved channel," *Physica A: Statistical Mechanics and* its Applications, vol. 553, p. 123979, 2020.

- [19] J. Akram, N. S. Akbar, and E. N. Maraj, "A comparative study on the role of nanoparticle dispersion in electroosmosis regulated peristaltic flow of water," *Alexandria Engineering Journal*, vol. 59, no. 2, pp. 943– 956, 2020.
- [20] A. Saleem, S. Akhtar, F. M. Alharbi, S. Nadeem, M. Ghalambaz, and A. Isskhov, "Physical aspects of peristaltic flow of hybrid nanofluid inside a curved tube having ciliated wall," *Results in Physics*, vol. 19, p. 103431, 2020.
- [21] U. M. Zahid, Y. Akbar, and F. M. Abbasi, "Entropy generation analysis for peristaltically driven flow of hybrid nanofluid," *Chinese Journal of Physics*, vol. 67, pp. 330–348, 2020.
- [22] A. Abbasi, F. Mabood, W. Farooq, and U. Khan, "Radiation and joule heating effects on electroosmosismodulated peristaltic flow of Prandtl nanofluid via tapered channel," *International Communications in Heat* and Mass Transfer, vol. 123, p. 105183, 2021.
- [23] A. P. Devaki, B. Venkateswarlu, S. Srinivas, and S. Sreenadh, "MHD peristaltic flow of a nanofluid in a constricted artery for different shapes of nanosized particles," *Nonlinear Engineering*, vol. 9, no. 1, pp. 51–59, 2019.
- [24] A. Mondal and G. C. Shit, "Transport of magnetonanoparticles during electro-osmotic flow in a micro-tube in the presence of magnetic field for drug delivery application," *Journal of Magnetism and Magnetic Materials*, vol. 442, pp. 319–328, 2017.
- [25] M. Rafiq, M. Sajid, S. E. Alhazmi, M. I. Khan, and E. R. El-Zahar, "MHD electroosmotic peristaltic flow of Jeffrey nanofluid with slip conditions and chemical reaction," *Alexandria Engineering Journal*, vol. 61, no. 12, pp. 9977–9992, 2022.
- [26] M. Ren, T. Zhang, J. Cui, X. Chen, and B. Wu, "Magnetofluid unsteady electroosmotic flow of Jeffrey fluid at high zeta potential in parallel microchannels," *Open Physics*, vol. 20, pp. 560–572, 2022.
- [27] R. Choudhari, H. Vaidya, K. V. Prasad, R. K. Gulab, K. Guedri, A. Rehman, and A. M. Galal, "Electroosmosis augmented MHD third-grade fluid with slip and variable properties: An application for blood flow in arteries," *Journal of Computational Biophysics and Chemistry*, 2022.
- [28] M. A. Nuwairan and B. Souayeh, "Simulation of gold nanoparticle transport during MHD electroosmotic flow in a peristaltic micro-channel for biomedical treatment," *Micromachines*, vol. 13, no. 3, p. 374, 2022.
- [29] Y. Akbar, H. Alotaibi, U. Javed, M. Naz, and M. M. Alam, "Electroosmotic modulated peristaltic transport of Carreau magneto-nanofluid with modified Darcy's law," Waves in Random and Complex Media, vol. 32, no. 6, 2022.
- [30] J. Akram, N. S. Akbar, and D. Tripathi, "Electroosmosis augmented MHD peristaltic transport of SWCNTs

- suspension in aqueous media," *Journal of Thermal Analysis and Calorimetry*, pp. 1–18, 2021.
- [31] T. Siva, S. Jangili, and B. Kumbhakar, "Heat transfer analysis of MHD and electroosmotic flow of non-Newtonian fluid in a rotating microfluidic channel: an exact solution," *Applied Mathematics and Mechanics*, vol. 42, pp. 1048–1062, 2021.
- [32] S. Noreen, S. Waheed, D. C. Lu, and A. Hussanan, "Heat measures in performance of electro-osmotic flow of Williamson fluid in micro-channel," *Alexandria Engineering Journal*, vol. 59, no. 6, pp. 4081–4100, 2020.
- [33] S. Noreen, Quratulain, and D. Tripathi, "Heat transfer analysis on electroosmotic flow via peristaltic pumping in non-Darcy porous medium," *Thermal Science and Engineering Progress*, vol. 11, pp. 254–262, 2019.
- [34] Imran, M. A. Z. Raja, M. Shoaib, M. Zeb, and K. S. Nisar, "Electro-osmotic transport of a Williamson fluid within a ciliated microchannel with heat transfer analysis," *Case Studies in Thermal Engineering*, 2023.
- [35] S. Deng, M. Li, Y. Yang, and T. Xiao, "Heat transfer and entropy generation in two-layered electroosmotic flow of power-law nanofluids through a microtube," *Applied Thermal Engineering*, vol. 196, p. 117314, 2021.
- [36] R. Sun, W. Hu, B. Jiao, and C. Qi, "Heat transfer characteristics and entropy generation of electroosmotic flow in a rotating rectangular microchannel," *International Journal of Thermal Sciences*, vol. 140, pp. 238–254, 2019.
- [37] Venkateswarlu and P. V. Satya Narayana, "Cu-Al2_22 O3_33/H2_22O hybrid nanofluid flow past a porous stretching sheet due to temperature dependent viscosity and viscous dissipation," *Heat Transfer*, vol. 50, no. 1, pp. 432–449, 2021.
- [38] Venkateswarlu and P. V. Satya Narayana, "Chemical reaction and radiation absorption effects on the flow and heat transfer of a nanofluid in a rotating system," *Applied Nanoscience*, vol. 5, no. 3, pp. 351–360, 2015.
- [39] H. Yasmin and N. Iqbal, "Convective mass/heat analysis of an electroosmotic peristaltic flow of ionic liquid in a symmetric porous microchannel with Soret and Dufour," *Mathematical Problems in Engineering*, pp. 1–14, 2021.
- [40] N. Iqbal, H. Yasmin, A. Bibi, and A. A. Attiya, "Peristaltic motion of Maxwell fluid subject to convective heat and mass conditions," *Ain Shams Engineering Journal*, vol. 12, no. 3, pp. 3121–3131, 2021.
- [41] P. Tamiharasi, R. Vijayaragaven, and A. Magesh, "Heat and mass transfer analysis of the peristaltic driven flow of nanofluid in an asymmetric channel," *Partial Differential Equations in Applied Mathematics*, vol. 4, p. 100087, 2021.
- [42] J. Iqbal, M. Abbasi, and A. Shehzad, "Heat transportation in peristalsis of Carreau-Yasuda nanofluid through a curved geometry with radial magnetic field," *International Communications in Heat and Mass Transfer*, vol. 117, p. 104774, 2020.
- [43] S. Waheed, S. Noreen, and A. Hussanan, "Study of heat and mass transfer in electroosmotic flow of third-order fluid through peristaltic microchannels," *Applied Sciences*, vol. 9, no. 10, p. 2164, 2019.
- [44] A. Mondal and G. C. Shit, "Electro-osmotic flow and heat transfer in a slowly varying asymmetric micro-channel

- with Joule heating effects," Fluid Dynamics Research, 2018.
- [45] J. Zheng and Y. Jian, "Rotating electroosmotic flow of two-layer fluids through a microparallel channel," *International Journal of Mechanical Sciences*, vol. 136, pp. 293–302, 2018.
- [46] A. Mallick, "Thermofluidic characteristics of electrokinetic flow in a rotating microchannel in presence of ion slip and Hall currents," *International Communications in Heat and Mass Transfer*, vol. 126, p. 105350, 2021.
- [47] X. Feng, X. Si, L. Cao, and B. Zhu, "The slip flow of generalized Maxwell fluids with time-distributed characteristics in a rotating microchannel," *Applied Mathematics Letters*, vol. 120, p. 107260, 2021.
- [48] M. Patel, K. S. S. Harish, and P. Kaushik, "Rotating electroosmotic flow of power-law fluid through polyelectrolyte grafted microchannel," *Colloids and Surfaces B: Biointerfaces*, vol. 193, p. 111058, 2020.
- [49] M. Xu and Y. Jian, "Unsteady rotating electroosmotic flow with time-fractional Caputo-Fabrizio derivative," *Applied Mathematics Letters*, vol. 100, p. 106015, 2020.
- [50] P. Liang, S. Wang, and M. Zhao, "Numerical study of rotating electroosmotic flow of Oldroyd-B fluid in a microchannel with slip boundary condition," *Chinese Journal of Physics*, vol. 65, pp. 459–471, 2020.
- [51] L. Cao, P. Zhang, B. Li, J. Zhu, and X. Si, "Numerical study of rotating electro-osmotic flow of double layers with a layer of fractional second-order fluid in a microchannel," *Applied Mathematics Letters*, vol. 111, p. 106633, 2021.
- [52] P. V. Satya Narayana and B. Venkateswarlu, "Heat and mass transfer on MHD nanofluid flow past a vertical porous plate in a rotating system," *Frontiers in Heat and Mass Transfer*, vol. 7, no. 1, pp. 1–10, 2016.
- [53] P. V. Satya Narayana, B. Venkateswarlu, and S. Venkataramana, "Thermal radiation and heat source effects on a MHD nanofluid past a vertical plate in a rotating system with porous medium," *Heat Transfer Asian Research*, vol. 44, no. 1, pp. 1–19, 2015.
- [54] P. V. Satya Narayana, B. Venkateswarlu, and S. Venkataramana, "Effects of Hall current and radiation absorption on MHD micropolar fluid in a rotating system," *Ain Shams Engineering Journal*, vol. 4, no. 4, pp. 843–854, 2013.

Appendix A

$$F_1 = \frac{\psi_1 - \psi_2 \sinh(kh_1)}{\cosh(kh_1)}$$

$$F_2 = \frac{\psi_1 \cosh(kh_2) - \psi_2 \cosh(kh_1)}{\sinh(kh_1)\cosh(kh_2) - \sinh(kh_1)\cosh(kh_2)}$$

$$F_3 = \frac{(1 + \lambda_1)C_o}{2N^2}$$

$$F_4 = \frac{-F_1(1+\lambda_1)}{k^2 - N^2}, F_5 = \frac{-F_2(1+\lambda_1)}{k^2 - N^2}$$

$$F_6 = N \sinh(Nh_1) + \frac{\beta_1}{1+\lambda_1} N^2 \cosh(Nh_1)$$

$$F_7 = N \cosh\left(Nh_1\right) + \frac{\beta_1}{1 + \lambda_1} N^2 \sinh\left(Nh_1\right)$$

$$F_8 = 2F_3h_1 + F_4k\sinh(kh_1) + F_5k\cosh(kh_1) + \frac{\beta_1}{1 + \lambda_1} \binom{2F_3 + F_4k^2\cosh(kh_1)}{+F_5k^2\sinh(kh_1)} + 1$$

$$F_9 = N \sinh(Nh_2) - \frac{\beta_2}{1 + \lambda_1} N^2 \cosh(Nh_2)$$
$$F_{10} = N \cosh(Nh_2) - \frac{\beta_2}{1 + \lambda_1} N^2 \sinh(Nh_2)$$

$$\begin{split} F_{11} &= 2F_3h_2 + F_4k\sinh\left(kh_2\right) + F_5k\cosh\left(kh_2\right) \\ &- \frac{\beta_2}{1 + \lambda_1} \Big(2F_3 + F_4k^2\cosh\left(kh_2\right) + F_5k^2\sinh\left(kh_2\right)\Big) + 1 \end{split}$$

$$F_{12} = h_1 - h_2, \quad F_{13} = \cosh(Nh_1) - \cosh(Nh_2)$$

 $F_{14} = \sinh(Nh_1) - \sinh(Nh_2)$

$$\begin{split} F_{15} &= F_3 \left(h_1^2 - h_2^2 \right) + F_4 \left(\cosh \left(k h_1 \right) - \cosh \left(k h_2 \right) \right) \\ &+ F_5 \left(\sinh \left(k h_1 \right) - \sinh \left(k h_2 \right) \right) - q \end{split}$$

$$F_{16} = \frac{F_{13}}{F_{12}}, \qquad F_{17} = \frac{F_{14}}{F_{12}}, \qquad F_{18} = \frac{F_{15}}{F_{12}},$$

$$F_{19} = F_6 - F_{16}, \qquad F_{20} = F_7 - F_{17}, F_{21} = F_8 - F_{18}$$

$$\begin{split} F_{22} &= F_9 - F_{16}, F_{23} = F_{10} - F_{17}, F_{25} = F_{11} - F_{18} \\ c_3 &= -\frac{F_{21} + F_{20}c_4}{F_{19}}, \qquad c_4 = \frac{F_{25}F_{19} - F_{21}F_{22}}{F_{20}F_{22} - F_{23}F_{19}} \end{split}$$

$$G_1 = -\frac{Br}{1 + \lambda}, \quad G_2 = -M^2 \text{ Pr},$$

$$G_3 = G_1c_3^2N^4 + G_2c_4^2N^2, G_4 = G_1c_4^2N^4 + G_2c_3^2N^2$$

$$G_5 = G_1 F_4^2 k^4 + G_2 F_5^2 k^2, G_6 = G_1 F_5^2 k^4 + G_2 F_4^2 k^2$$

$$G_7 = 2C_2 G_2 C_2 N + 4C_4 G_1 F_2 N^2$$

$$G_8 = 2C_2G_2F_4k + 4F_3G_1F_5k^2$$

$$G_9 = 2C_2G_2F_4k + 4F_3G_1F_5k^2$$

$$G_{10} = 2C_2G_2F_5k + 4F_3G_1F_4k^2$$

$$G_{11} = C_3 G_2 C_4 N^2 + C_3 G_1 C_4 N^4, \ G_{12} = 4C_3 G_2 F_3 N$$

$$G_{13} = 2C_3G_2F_4kN + 2C_4G_1F_5k^2N^2$$

$$G_{14} = 2C_3G_2F_5kN + 2C_4G_1F_4k^2N^2$$

$$G_{15} = 2C_4G_2F_4kN + 2C_3G_1F_5k^2N^2$$

$$G_{16} = 2C_4G_2F_5Nk + 2C_3G_1F_4N^2k^2$$

$$G_{17} = F_4 F_5 G_2 k^2 + F_4 F_5 G_1 k^4, G_{18} = 4F_3^2 G_2$$

$$G_{19} = 2C_2G_2F_3, G_{20} = 4C_4G_2F_3N$$

$$G_{21} = 4F_3G_2F_4k, G_{22} = 4F_3G_2F_5k,$$

$$G_{23} = 4F_3^2 G_2 + G_2 C_2^2, G_{24} = \frac{G_3}{8N^2} + \frac{G_4}{8N^2}$$

$$G_{25} = \frac{G_5}{8k^2} + \frac{G_6}{8k^2}, G_{26} = \frac{G_7}{N^2} + \frac{2G_{20}}{N}$$

$$G_{27} = \frac{G_8}{N^2} + \frac{2G_{12}}{N}, G_{28} = \frac{G_9}{k^2} + \frac{2G_{22}}{k}$$

$$G_{29} = \frac{G_{10}}{k^2} + \frac{2G_{21}}{k}, G_{30} = \frac{G_{11}}{4N^2}, G_{31} = \frac{G_{12}}{N^2}$$

$$G_{32} = \frac{G_{13}}{N^2} + \frac{1}{k^2} + \frac{2G_{16}}{kN}, \quad G_{33} = \frac{G_{16}}{N^2} + \frac{1}{k^2} + \frac{2G_{13}}{kN}$$

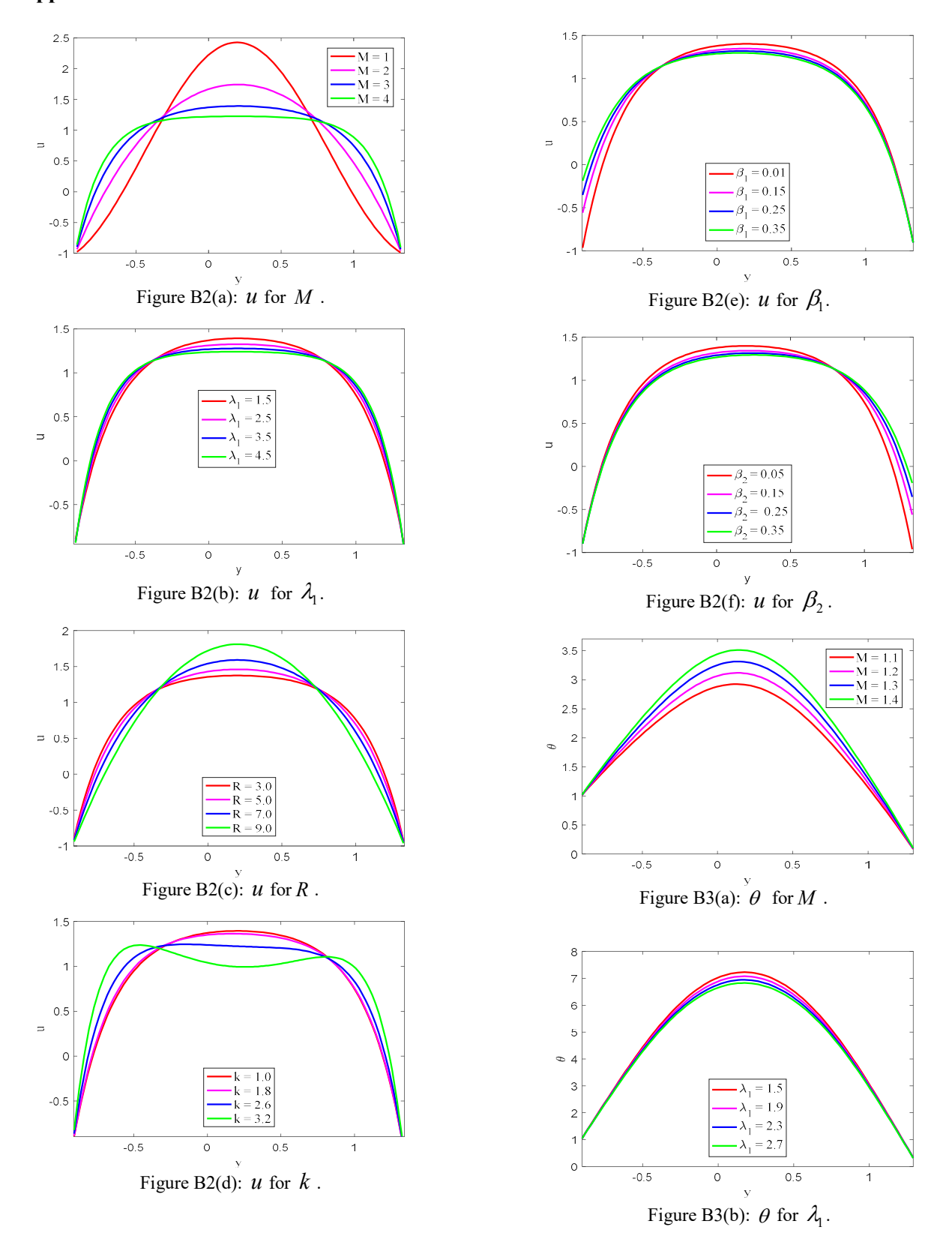
$$G_{34} = \frac{G_{14}}{N^2} + \frac{1}{k^2} + \frac{2G_{15}}{kN}, \qquad G_{35} = \frac{G_{15}}{N^2} + \frac{1}{k^2} + \frac{2G_{14}}{kN}, \qquad G_{36} = \frac{G_{17}}{4k^2}, \qquad G_{37} = \frac{G_{20}}{N^2}$$

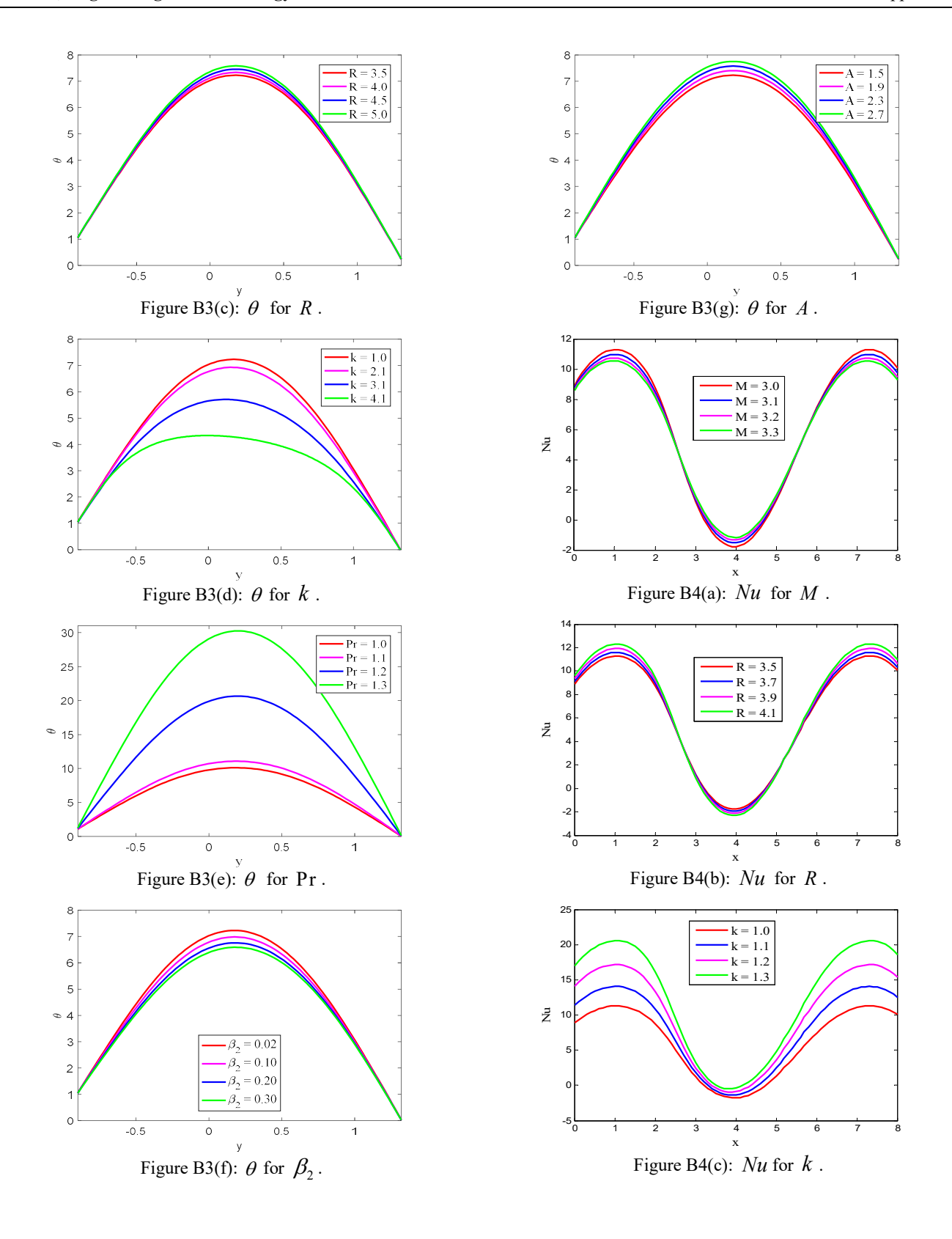
$$G_{38} = \frac{G_{21}}{k^2}, G_{39} = \frac{G_{22}}{k^2}, G_{42} = \frac{G_{18}}{12}$$

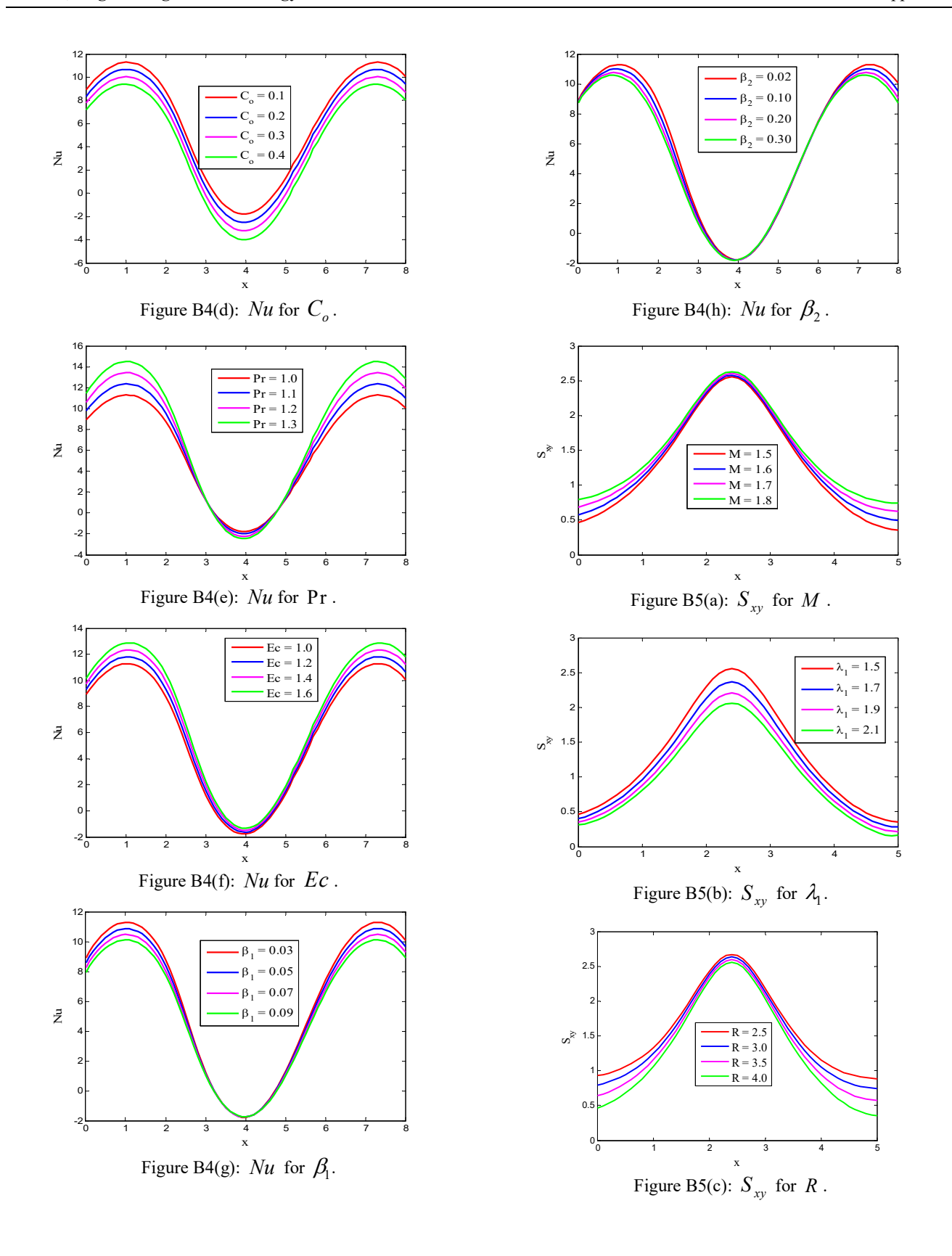
$$G_{41} = \frac{G_{19}}{6}, G_{40} = \frac{G_3}{4} - \frac{G_4}{4} + \frac{G_5}{4} - \frac{G_6}{4} + \frac{G_{23}}{2}$$

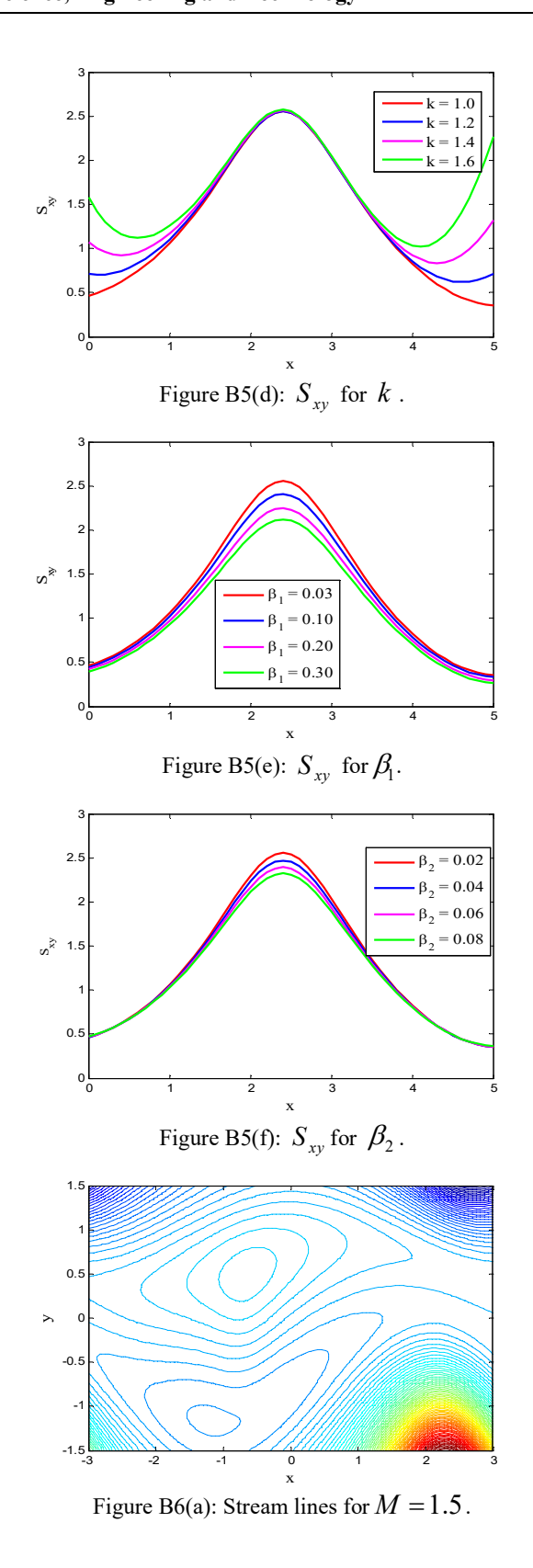
$$\begin{aligned} G_{4i} &= G_{3i} \left\{ \cosh(2Nh_i) - \right\} + G_{2i} \left\{ \cosh(2kh_i) - \right\} \\ &+ G_{2i} \left\{ \sinh(Nh_i) - \right\} \\ &+ G_{3i} \left\{ h_i \cosh(Nh_i) - \right\} \\ &+ G_{3i} \left\{ h_i \sinh(Nh_i) - \right\} \\ &+ G_{3i} \left\{ h_i h_i + \left\{ h_i h_i - h_i \right\} \\ &+ G_{$$

Appendix B









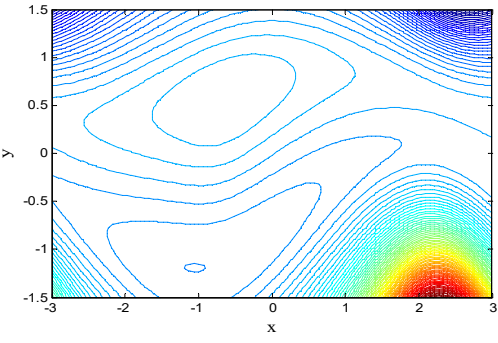


Figure B6(b): Stream lines for M = 1.6.

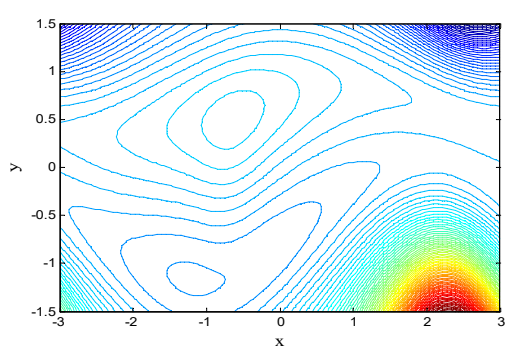


Figure B6(c): Stream lines for $\lambda_1 = 1.5$.

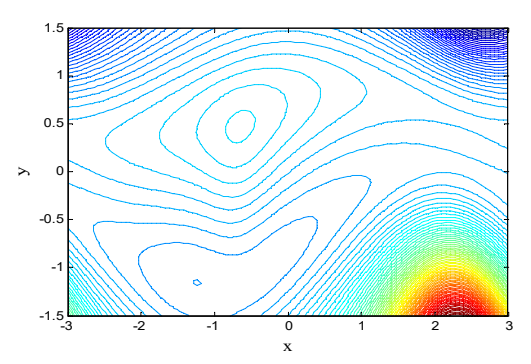


Figure B6(d): Stream lines for $\lambda_1 = 1.6$.